



Human body stimuli-responsive flexible polyurethane electrospun composite fibers-based piezoelectric nanogenerators

Kandiyil Juraij¹, V. H. Shafeeq², Akash M. Chandran³, Suni Vasudevan¹, Prasanna Kumar S. Murali², and Athiyathil Sujith^{1,*}

¹Materials Research Laboratory, Department of Chemistry, National Institute of Technology Calicut, Calicut 673601, India

²Department of Metallurgical Engineering and Materials Science, Indian Institute of Technology Bombay, Mumbai 400076, India

³Materials Chemistry and Polymer Technology Group, Department of Chemical Engineering, National Institute of Technology Calicut, Calicut 673601, India

Received: 10 October 2022

Accepted: 12 December 2022

Published online:

1 January 2023

© The Author(s), under exclusive licence to Springer Science+Business Media, LLC, part of Springer Nature 2022

ABSTRACT

Piezoelectric materials derived from piezoelectrically inactive polymers and lead-free functional nanofillers have received a lot of attention for their ability to convert mechanical energy associated with various human body movements into electrical signals. Herein, the fabrication and performance of a novel thermoplastic polyurethane/nanohydroxyapatite electrospun composite membrane-based piezoelectric nanogenerator (PENG) is using polydimethylsiloxane (PDMS). The nanohydroxyapatite (nHA) and oxidized multiwalled carbon nanotube (o-MWCNT) fillers converted a non-piezoelectric PU polymer material into a piezoelectrically active composite material. Compared to pristine electrospun PU, every composite sample showed improved mechanical properties, thermal stability, dielectric properties, and piezoelectric characteristics. Dynamic-contact electrostatic force microscopy (DC-EFM) confirmed the piezoelectric characteristics of all composite samples. The nHA/o-MWCNT hybrid filler-modified optimized nanofibrous sample (PHAT) showed outstanding dielectric properties and piezoelectric characteristics. The PHAT-based PENG showed the highest stimuli-responsive output voltage in the 0.4–32 V range, whereas the pristine electrospun PU-based PENG showed only an output voltage of 0.08–5.75 V from various stimuli. The flexible PU electrospun composite membrane can be considered a new potential material for harvesting electrical energy from the mechanical energy associated with various human body motions.

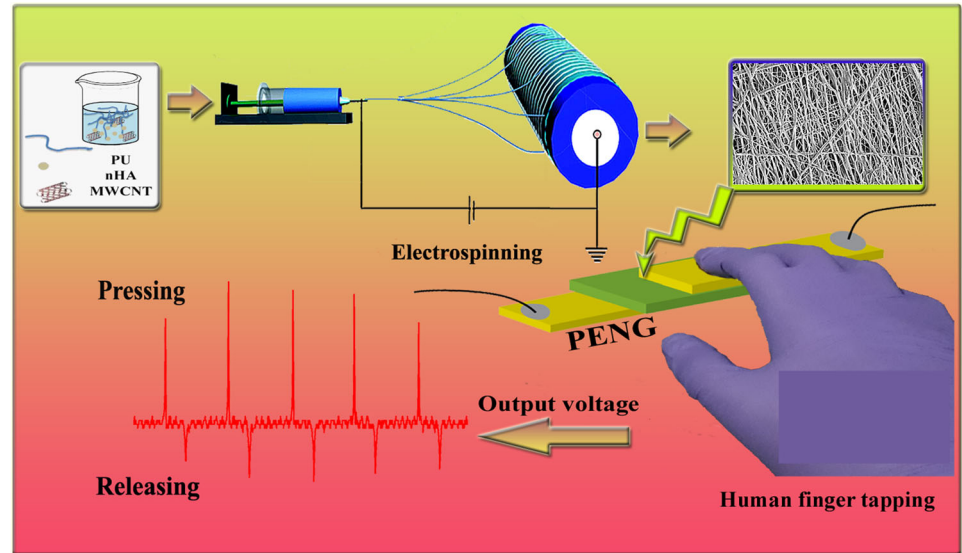
Handling Editor: Kevin Jones.

Address correspondence to E-mail: athiyathil.sujith@gmail.com

E-mail Address: juraijkdy@gmail.com

<https://doi.org/10.1007/s10853-022-08086-8>

GRAPHICAL ABSTRACT



Introduction

The energy crisis is a major concern in the contemporary age due to the tremendous increase in the loss of fossil-based natural resources [1]. Limited supply and increased consumption of fossil fuels such as oil, coal, and gases lead to an unbalanced state between energy supply and demand [2]. In the past decade, sustainable energy resources such as wind energy, hydroelectric power, wave energy, solar energy, biomass energy, and tidal energy have gained much attention [3]. As a consequence of the downsizing of portable and wireless electronics, new power sources have become essential for modern smart devices and systems [4]. The deployment of piezoelectric nanocomposites as a reliable and straightforward method for mechanical energy harvesting has received a lot of interest in this context [5].

Piezoelectric materials can produce electrical energy by applying mechanical stress [6]. Many materials have been discovered to be quite useful in the development of piezoelectric materials. Inorganic materials such as quartz, zinc oxide (ZnO), cadmium sulfide (CdS), and lead titanate-zirconate (PbTiO_3 – PbZrO_3 PZT) have been extensively studied as

piezoelectric materials [7, 8]. Some of them include lead, which has an adverse impact on organisms and the ecosystem. Lead-free piezoelectric functional materials, such as langasite, tungsten bronze-based material, and bismuth layer-structured ferroelectrics (BLSF), can be better options for energy harvesting than the currently used lead-based piezoelectric materials [9]. Perovskite-based ceramics, such as barium titanate (BaTiO_3), their hybrid derivatives, and their aqueous solutions, have also been investigated recently [10]. Despite the fact that several piezoelectric ceramics have been produced, their hard and brittle properties limit their usage as smart energy harvesters. To overcome this problem, flexible polymers are widely used [11]. Poly(vinylidene fluoride) (PVDF) is a well-known and extensively studied piezoelectric polymer [12–15]. Based on the molecular chain conformation, its phases are classified as α , β , γ , and δ . The presence of the β phase is responsible for the piezoelectric property due to its highest dipole moment per unit volume [16].

The introduction of piezoelectric properties into a non-PVDF polymer matrix has great significance. Thermoplastic polyurethane (TPU) is a semicrystalline, dielectric, and elastomeric polymer made up of hard and soft segments [17]. It possesses high

elasticity, good weather resistance, impact resistance, and abrasion resistance [18]. Even though it has a low dielectric constant (ϵ'), the incorporation of conductive functional nanofillers such as carbon nanotubes and graphene could increase the dielectric properties [17]. Since TPU has excellent flexibility, it can be considered for fabricating wearable devices for dielectric and other allied applications. In order to impart piezoelectric properties to TPU, strategies such as blending, surface functionalization, and composite formation are adopted [19]. A few efforts have been made to impart piezoelectric property into the PU by blending it with PVDF. Bin et al. [20] fabricated a piezoelectric blend system of polyurethane (PU) and polyvinylidene fluoride-trifluoroethylene (PVDF-TrFE). On the other hand, many efforts have been made to develop piezoelectric polymer blend systems using non-PVDF polymers other than TPU and piezoelectrically active PVDF [21]. Sengupta et al. [22] prepared a PVDF-polycarbazole electrospun membrane for enhanced piezoelectric performance. It enhanced the β phase content and thereby enhanced piezoelectric action without compromising the flexibility of samples. Kalifa et al. [23] fabricated a polyaniline-halloysite nanotube-based PVDF blend membrane with a maximum output voltage of 7.2 V.

Due to the phase separation of polymers in polymer blends, polymer composites with piezoelectric active fillers have been considered a promising solution to fabricate wearable, implantable, and flexible piezoelectric smart materials [24]. Through the judicious selection of piezoelectrically active fillers, it is possible to manufacture highly flexible piezoelectric composite materials. This study used nanohydroxyapatite (nHA) and oxidized MWCNT (o-MWCNT) as functional fillers. Hydroxyapatite is an inorganic mineral that occurs naturally and has the chemical formula $\text{Ca}_{10}(\text{PO}_4)_6\text{OH}_2$. Dry bone is composed of 60–70% hydroxyapatite, as well as some protein and inorganic salts [25]. Synthetic hydroxyapatite (HAp) and nHA have been used instead of naturally generated hydroxyapatite without affecting bioactivity or crystalline characteristics [26–28]. Recently, nHA has gained much deliberation as a dielectric and lead-free piezoelectric material [29, 30]. It has a negatively charged c plane and a positively charged a plane that can produce orientation or dipolar polarization. The dielectric, piezoelectric, or ferroelectric properties of materials are governed by

polarization, such as orientation (dipolar), ionic, electronic, or interfacial space charge [31].

Among various composites, electrospun composite membranes have gained much interest due to their large surface-to-volume ratio, high porosity, ease of surface functionalization, and uniform load transfer upon the application of mechanical stress [32, 33]. Electrospun fibers are generated by a technique called electrospinning. In this process, the polymer solution or melt is drawn electrostatically by applying a high electric field as a polymer jet. The polymer jet is drawn to a mandrel by a whipping motion and collected over it in the form of continuous fibrous mats [34]. Compared to conventional macro-structural films or sheets, the nano-structured membranes can effectively convert mechanical energy associated with mild movements into piezoelectricity. Moreover, electrospun composite fibers can show a net nonzero dipole moment due to the coaxial orientation of the dipoles generated by polar functional groups of polymers along the fiber axis [21]. Thus, electrospinning is a technique of choice for fabricating sensitive piezoelectric devices [35]. A few researchers have attempted to introduce piezoelectric properties to non-piezoelectric polymers using an electrospun composite preparation strategy. Bairagi et al. [36] prepared polyacrylonitrile (PAN)/copper oxide (CuO) nanorods-based electrospun composite membranes as piezoelectric nanogenerators. Even though it showed an output voltage of 5 V from human finger tapping, there was no attempt to confirm the piezoelectricity using a specific characterization. Shafeeq et al. [37] developed a piezoelectric material using a non-piezoelectric ethylene-co-vinyl acetate and rubbery polyurethane polymer blend system by incorporating nHA as the piezoelectric filler. Even though it has appreciable ferro-piezoelectric properties, it could not produce a sufficient output voltage during various stimuli. Moreover, no fine fiber morphology has been observed from the electrospun membrane due to the presence of a rubbery polymer blend system. The present study uses dielectric thermoplastic polyurethane as a polymer matrix instead of a blended system.

Although a few articles investigated the improvement of the dielectric properties of TPU, none of them explored the piezoelectric performance of TPU/nanohydroxyapatite-based electrospun composites [38–42]. This study presents a novel piezoelectric polyurethane/nanohydroxyapatite-based

electrospun composite membrane as a stimuli-responsive piezoelectric nanogenerator. The effects of functional fillers (nHA and o-MWCNT) on the dielectric, piezoelectric, and mechanical properties of electrospun PU have been thoroughly investigated. Moreover, simple piezoelectric nanogenerators (PENGs) have been fabricated using PU-based electrospun composite membranes. Thus, the major purpose of this study is to develop thermoplastic polyurethane-based piezoelectric nanogenerators that respond to human body motions.

Materials and methods

Materials

TECOFLEX™ EG-85A grade thermoplastic polyurethane (TPU) ($M_w \approx 120,604$ g/mol) was supplied by Lubrizol Advanced Materials, Massachusetts, USA. The oxidized MWCNT (o-MWCNT) was purchased from Adnano Technologies, Pvt. Ltd., India. As per the production details, the outer and inner diameters of o-MWCNT are 10–30 nm and 5–10 nm, respectively. The nanohydroxyapatite (nHA) was prepared in the laboratory in accordance with the reported wet chemical method (Supplementary information S1) [28, 43]. Merck Pvt. Ltd., India, supplied polydimethylsiloxane (PDMS) (Sylgard 184), calcium nitrate tetrahydrate ($\text{Ca}(\text{NO}_3)_2 \cdot 4\text{H}_2\text{O}$), 99%, ammonium hydroxide (NH_4OH) (28% NH_3 in H_2O , $\geq 99\%$ trace metals basis), and diammonium hydrogen orthophosphate ($(\text{NH}_4)_2\text{HPO}_4$), $\geq 98\%$. Avra Chemicals, India, provided the solvents dimethylformamide (DMF), 99%, and tetrahydrofuran (THF), 99.5%. Copper foil and metallic wires for PENG fabrication were brought from the local market. A syringe ($21\text{G} \times 1''$) for electrospinning purposes was purchased from BD Emerald™.

Table 1 Formulations of samples

Sample	PU (%)	nHA (%)	o-MWCNT (%)
PU	100	0	0
PHA1	99.8	0.2	0
PHA2	99.6	0.4	0
PHAT	99.6	0.2	0.2

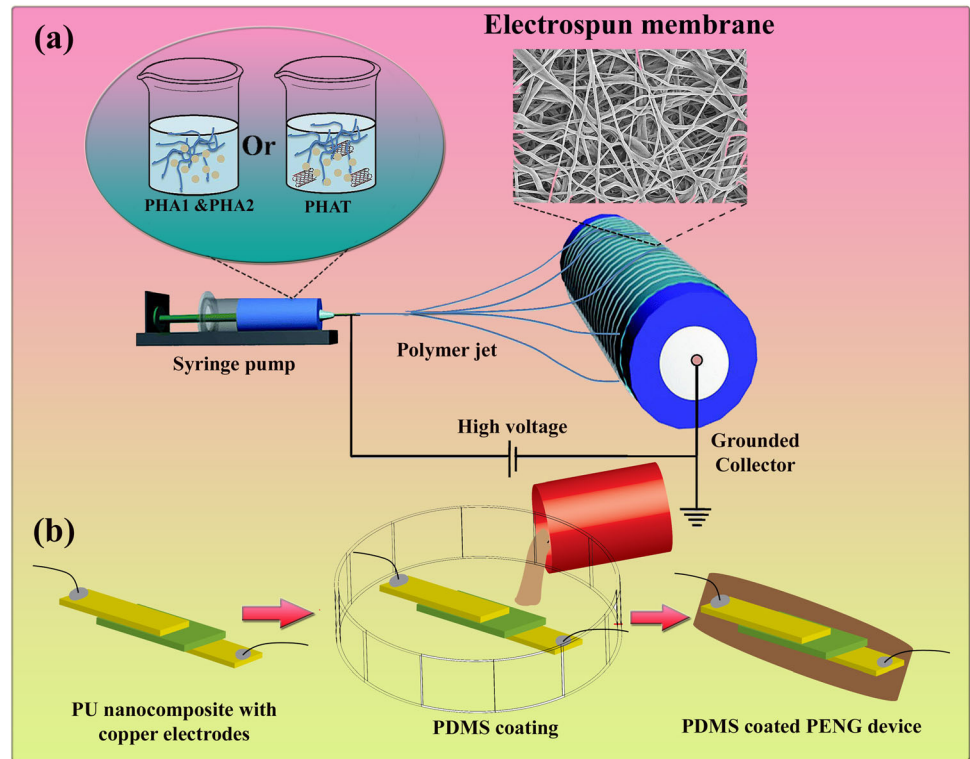
Preparation of electrospun composite membranes

The electrospinning solutions were primarily made by taking a total amount of 10 wt% polymer and filler in a THF:DMF (7:3) system, as shown in Table 1. PU/nHA spinning solutions were prepared by dispersing a specific amount of nHA (0.2–0.4%) in 3 mL of DMF and 7 mL of THF by ultrasonication for 30 min. To the resultant nHA dispersion, a suitable amount of PU pellets (99.6–99.8%) was added and placed for 6 h of stirring for complete dissolution. For the preparation of the nHA/o-MWCNT-modified composite sample (PHAT), 0.2% of the o-MWCNT was dispersed in 3 mL of DMF and 7 mL of THF by ultrasonication for 30 min. To the o-MWCNT dispersion, 0.2% of nHA was added and placed for another 30 min of ultrasonication. 99.6% of the PU was gently added to the nHA/o-MWCNT dispersion and stirred for 6 h to ensure complete dissolution. The prepared spinning solutions were filled into a 10-mL syringe with a metallic needle of 0.514 mm inner diameter ($21\text{G} \times 1''$). The syringe was connected to a high-voltage supply electrode mounted on a syringe pump (0–30 kV, HO-NFES-041 Holmarc, India). The other electrode was connected to a rotating mandrel with a 500 rpm rotational speed. The electrospinning processing parameters, such as the applied voltage, flow rate, and working distance, were fixed at 16 kV, 1.5 mL/hr, and 16 cm, respectively. The electrospinning process (Fig. 1a) of the 15 mL polymer solution was prolonged for another 10 h to achieve the requisite membrane thickness. The nanofibrous membranes were subjected to vacuum drying for 24 h to remove excess solvent.

Piezoelectric nanogenerators (PENGs) fabrication

The piezoelectric nanogenerators were fabricated using electrospun samples (PU, PHA1, PHA2, and PHAT). The electrospun membrane, measuring 0.154 mm in thickness, was shaped into a 2×2 cm² dimension and sandwiched between two copper electrodes. Copper wires were soldered to the two electrodes to connect them to the open circuit for the output voltage measurement. Finally, the fabrics were encapsulated using polydimethylsiloxane (PDMS) to generate PENGs. Figure 1b shows the schematic representation of PENG fabrication.

Figure 1 Schematic representation of **a** electrospinning of samples, **b** fabrication of piezoelectric nanogenerators (PENGs).



Characterization

Fourier transform infrared spectroscopy (FT-IR, Jasco FT/IR-4700) with a maximum resolution of 0.4 cm^{-1} and a signal-to-noise ratio of 35,000:1 was used to confirm the existence of functional groups and chemical bonds in ATR mode. With base correction, three scans were performed in the range of $4000\text{--}400\text{ cm}^{-1}$ for each sample. A field emission scanning electron microscope (FE-SEM) (Zeiss, Ultra 55) equipped with energy-dispersive spectroscopy (EDS) was used to investigate the morphology and elemental composition of all samples at an accelerating voltage of 5 kV. The average fiber diameter was calculated using ImageJ software. Raman spectroscopy (Horiba LabRam Confocal Raman Spectrometer, 532-nm laser) was used to validate o-MWCNT functionalization. It is a mirror-based spectrometer with an 800 mm focal length (600 holographic gratings, 1800 grooves/mm) and a scanning range of $50\text{--}4000\text{ cm}^{-1}$. TGA (Q-50, TA instruments) was used to evaluate the thermal properties of membranes. The experiment was performed between 0 and $600\text{ }^{\circ}\text{C}$, with a scan rate of $10\text{ }^{\circ}\text{C}/\text{min}$. The mechanical characteristics of the $1 \times 7\text{ cm}^2$ membranes were examined using a

Universal Testing Machine (UTM, Shimadzu Autograph, AG-Xplus series) with a 10 N applied stress. Dynamic-contact electrostatic force microscopy (DC-EFM) was used to investigate the piezoelectric–ferroelectric properties of electrospun composite samples (AFM, Park XE100). To monitor the hysteresis curves based on the EFM amplitude and phase, the samples were subjected to a voltage sweep from -10 to $+10\text{ V}$. An impedance analyzer (Wayne Kerr WK6500B) was used to investigate the dissipation factor ($\tan \delta$) and dielectric constant (ϵ'). The experiment was carried out by placing samples with a thickness of 0.154 mm and a diameter of 10 mm between copper electrodes.

PENG device characterization

A digital storage oscilloscope (Tektronix, TBS 2000 series) was used to examine the output voltage of fabricated PENGs. The devices were subjected to an impact force test with an impact force of 1.73 N to demonstrate the energy harvesting performance [44]. A home-built impact force setup was used for this. A metallic object of $4.52 \times 10^{-4}\text{ m}^2$ contact area weighing 176.880 g was dropped from a known distance of 1 m , and the generated output voltage was measured

using a digital oscilloscope. Detailed information about the impact force test is given under Supplementary information S2. Moreover, a home-built tapping machine (Fig.S2) was used to investigate the output voltage generated by tapping at a controlled frequency and area. A finger-tapping procedure and the impact of various human body joint bendings were used as the human body-based mechanical energy sources for generating electrical energy. For calculating current (I), power (P), current density (J), and power density (P_d), a 1-M Ω resistor was introduced into the circuit, and the output voltage was measured. Equations for calculating current, power, current density, and power density are given under Supplementary information S3.

Results and discussion

Fiber morphology and elemental mapping

A nanostructured membrane can show enhanced piezoelectric performance compared to macro-

structural films. Nanofiber morphology and size regulation by electrospinning have great importance. Figure 2a and b–d shows the SEM micrographs of electrospun polyurethane and electrospun composite membranes, respectively. A TEM image of nanohydroxyapatite is given under Supplementary information S4 (Fig. S3). It showed a rod-like structure with an average length of 82.96 nm and an average width of 22.91 nm.

Electrospun PU shows a large fiber diameter of 829 ± 32 nm with a cylindrical, interconnected morphology. nHA and o-MWCNT fillers incorporation caused a large decrease in the fiber diameter. Samples PHA1 and PHA2 showed fiber diameters of 497 ± 34 nm and 324 ± 33 , respectively, whereas sample PHAT showed the lowest fiber diameter of 284 ± 31 nm. The gradual decrease in the fiber diameter was due to the enhanced electrical conductivity of composite solutions. Conductive fillers such as nHA and CNT can increase the charge density carried by the polymer solution; hence, it can enhance the stretching of the polymer jet, resulting in the formation of narrow fibers during the whipping

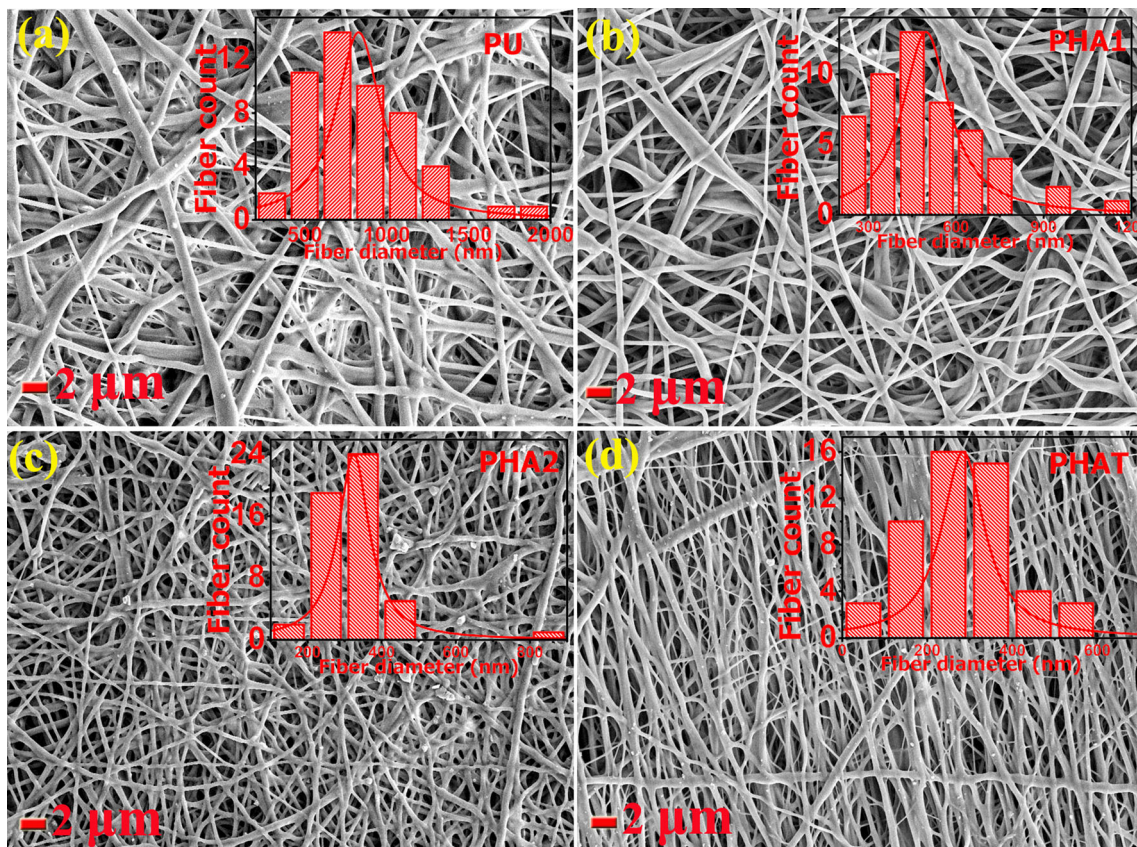


Figure 2 SEM micrographs and fiber diameter distributions of a pristine electrospun PU, b PHA1, c PHA2, d PHAT.

motion in the flight time [45]. Samples PHA1 and PHA2 showed randomly oriented and interconnected fiber morphology, whereas PHAT showed comparatively collinearly aligned fiber morphology. It was due to the excellent jet elongation and repulsion between charged polymer jets. Parallel polymer jets were generated during the whipping motion, and thin solid fibers were deposited on the collector without much overlap [46]. Because of the increased friction area, the aligned fiber morphology can offer an increased electrical output of the piezoelectric nanogenerators (PENGs) than those based on randomly oriented fiber webs [47]. This is further proved by the open-circuit voltage output of the PHAT composite-based PENG.

The energy-dispersive X-ray spectroscopy (EDS) spectra of electrospun PU, PHA1, PHA2, and PHAT samples are shown in Fig. S4. In the pristine electrospun PU, phosphorous (P) and calcium (Ca) were absent. As nHA loading increased, the amount of P and Ca was found to be increased from PHA1 to PHA2. Since PHA1 and PHAT samples had similar nHA input loadings, the final amounts of P and Ca in the composites were close to each other. The slight difference in the amount of Ca and P compared to the input filler loading was due to the loss of filler contents during electrospinning [48]. The presence of nanohydroxyapatite in the electrospun sample (PHA2) was further confirmed by elemental mapping. Figure 3b–f shows the elemental mapping of C, N, O, Ca, and P, respectively. It ensured the uniform distribution of nHA in the samples.

Bonding and crystalline characteristics

The FTIR spectra of nanofibrous PU, nHA, and PU/nHA nanofibrous composites are given in Fig. 4a. Due to the N–H group stretching, the pristine electrospun PU membrane exhibited a prominent peak at 3325 cm^{-1} . Peaks at $1690\text{--}1716\text{ cm}^{-1}$, respectively, represent intermolecular hydrogen-bonded C=O stretching and bare carbonyl stretching (C=O) [45]. The characteristic peaks of nHA were visible at 3566 cm^{-1} , 1024 cm^{-1} , 961 cm^{-1} , and 560 cm^{-1} , corresponding to the nHA structural OH^- ion stretching, PO_4^{3-} asymmetric stretching, PO_4^{3-} symmetric stretching, and out-of-plane bending of PO_4^{3-} , respectively [49]. Compared to the pristine electrospun PU, only hydrogen-bonded C=O stretching frequency was observed in all electrospun composite samples and all composites marked a peak shift from 1716 to 1697 cm^{-1} (Fig. 4b). This significant peak shift in the composites may be due to the stabilized hydrogen bonding between the $-\text{OH}$ group of nHA and the C=O functional groups of the PU [50]. Also, it may be due to the electrostatic interaction between Ca^{2+} ions present in nHA and the C=O functional groups of the PU [51]. Moreover, the enhanced intensity of the C=O peaks in the PU/nHA electrospun composites further confirmed the presence of additional hydrogen bonding, which may lead to stronger organic–inorganic interfacial interactions [52]. A possible interaction between nHA and PU is shown in Fig. 4c. All the characteristic peaks of nHA were visible in all composites. The intensity of the

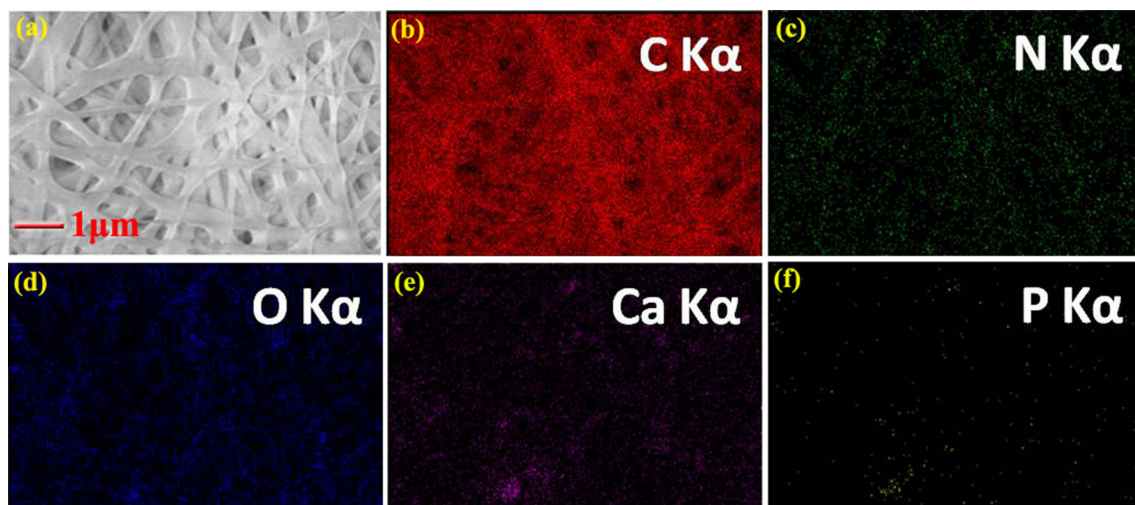


Figure 3 a Elemental mapping location from the SEM. Elemental mapping of nHA-loaded composite (PHA2), b carbon, c nitrogen, d oxygen, e calcium, f phosphorous.

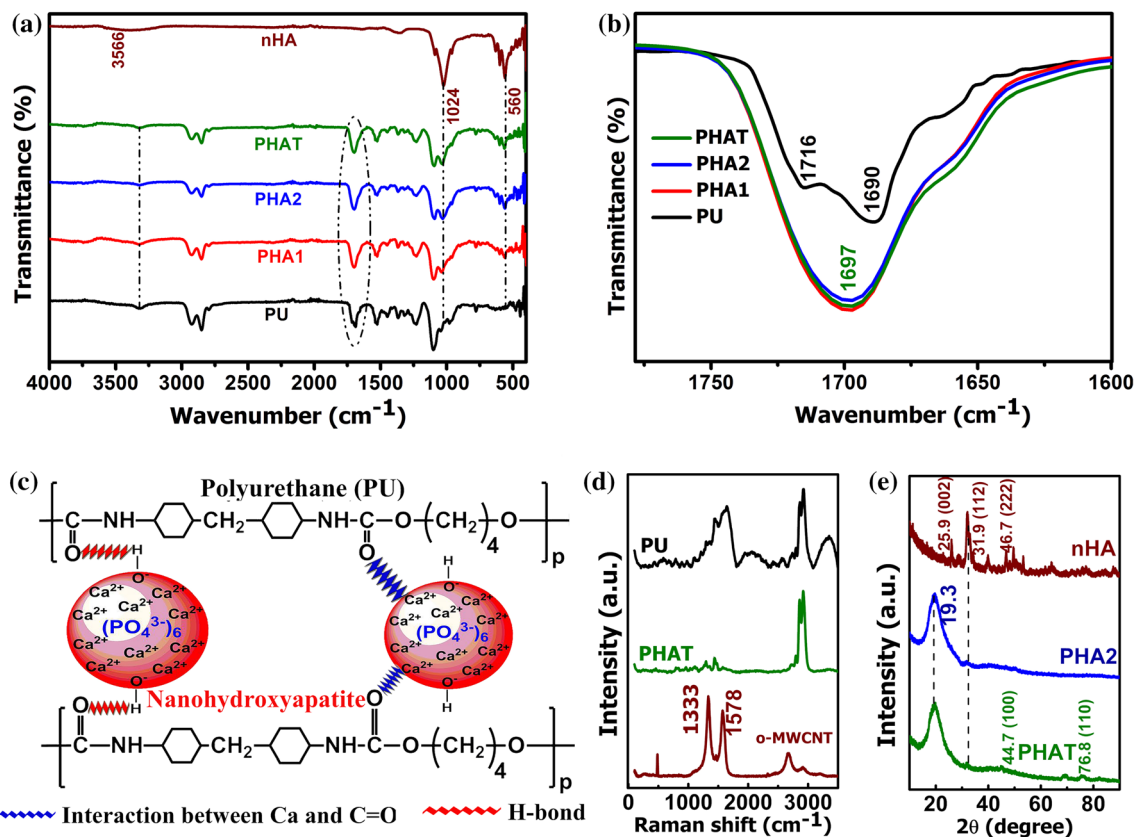


Figure 4 **a** FTIR spectra of nanohydroxyapatite, electrospun PU, and electrospun composites, **b** enlarged FTIR spectral peak of carbonyl stretching of electrospun PU and electrospun composite

peaks at 1024–560 cm^{-1} was increased in the composites compared to the pristine PU, which confirmed the proper modification of PU by nHA.

Figure 4d shows the Raman spectra of o-MWCNT, electrospun PU, and an o-MWCNT-modified electrospun composite sample (PHAT). The *D* band is represented by an absorption peak at 1333 cm^{-1} , while the *G* band is represented by an absorption peak at 1578 cm^{-1} . These significant peaks in the PHAT samples and their peak shift revealed that o-MWCNT successfully modified electrospun PU, and it further confirmed the nanocomposite formation [53].

Figure 4e shows the XRD patterns of the nHA and PU electrospun composite samples. nHA showed its prominent peaks at 25.95°, 31.9°, and 46.7°, corresponding to (022), (112), and (222) planes, respectively. It was consistent with JCPDS card number 01-072-1243 (Fig. S5) [54]. A less intense, prominent band ($2\theta = 31.9^\circ$) of nHA in the samples PHA2 and PHAT further confirmed the proper modification of

membranes at different nHA loadings, **c** proposed interaction between nHA and PU, **d** Raman spectra of samples, **e** XRD pattern of samples.

PU by nHA. These samples showed another peak at $2\theta = 19^\circ$, which was due to the semicrystalline nature of the PU backbone. In the PHAT membrane, two peaks were visible at 44.7°–76.8°, and it was due to the proper functionalization of PU by o-MWCNT.

Thermal and mechanical properties

Thermogravimetric analysis (TGA) and derivative thermogravimetric analysis (DTG) are shown in Fig. 5a and b, respectively. Both electrospun PU and electrospun composite membranes have two steps of degradation. The initial weight loss was caused by the decomposition of the peptide bond in the hard segment, whereas the second weight loss was caused by the breakage of the ether bond in the soft segment [55]. No significant weight loss was observed for nHA. Compared to the pristine fibrous PU membrane, the onset and T_{max} temperatures of all composite samples were much higher, showing the composites' superior thermal stability (Table 2).

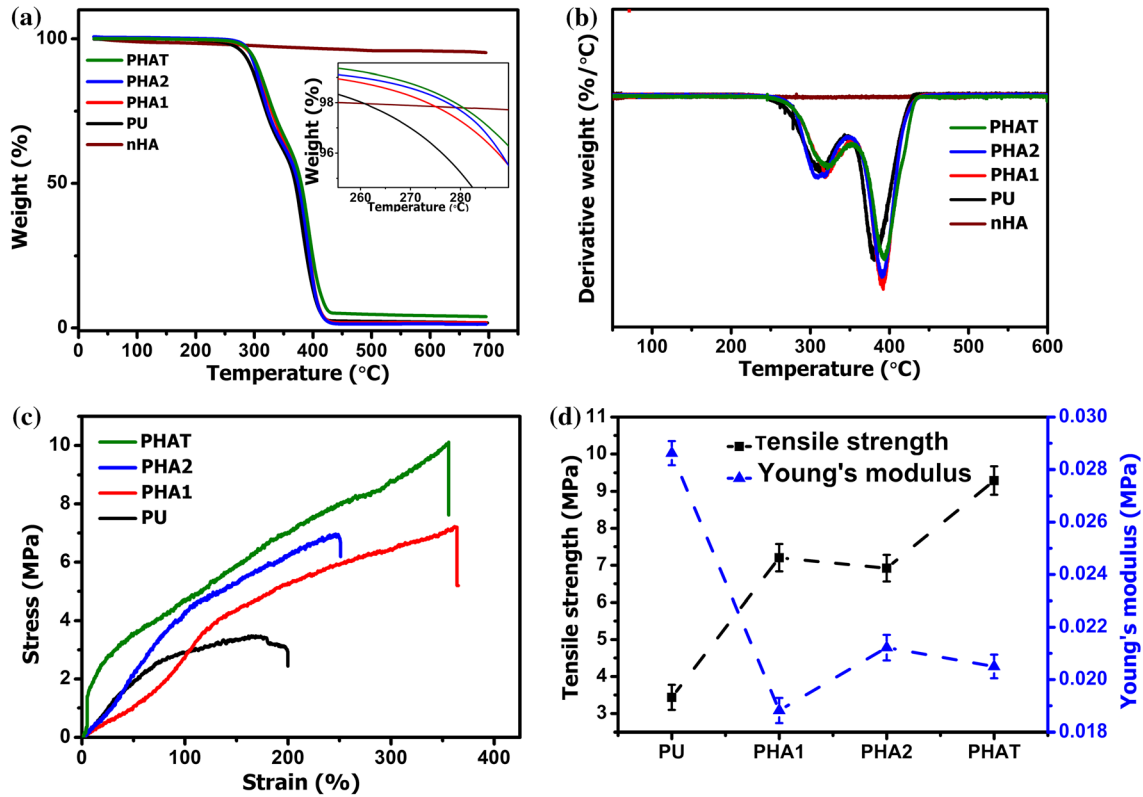


Figure 5 a TGA curves of samples, b DTG curves of samples, c stress–strain curves of electrospun membranes, d tensile strength and Young’s modulus of fibrous membranes.

Table 2 TGA data of samples

Sample	T_{onset} (°C)	T_{max1} (°C)	T_{max2} (°C)
PU	243	301	377
PHA1	289	307	388
PHA2	290	316	390
PHAT	294	324	393

Materials with high mechanical properties and flexibility are highly demanded in the fabrication of PENGs. Such materials could tolerate the impact forces applied during energy harvesting. The stress–strain curves of all samples are shown in Fig. 5c. Except for the PHAT sample, all electrospun membranes exhibit a nonlinear primary elastic region due to the slipping tendency of randomly oriented nanofibers over others [56, 57].

Electrospun PU showed the least tensile strength (3.4 MPa) and elongation at break (199%). Compared to virgin electrospun PU, even the nHA-alone modified PU electrospun membranes (PHA1 and PHA2) showed improved tensile strength and percentage

elongation. The nHA/o-MWCNT-modified PHAT sample showed the highest tensile strength (10.11 MPa). As the SEM image of the PHAT showed, electrospun fibers were sufficiently aligned compared to all other samples. Aligned electrospun fibers can resist the initial tensile load due to the uniaxial alignment of fibers along the applied stress direction; hence, they can uniformly distribute tensile stress among all fibers [58]. Moreover, the presence of MWCNT in the PHAT could impart high tensile strength and percentage elongation. However, compared to the PHA1 sample, the PHAT showed a slight reduction in the elongation at break. It may be due to the aggregation of nanoparticles at higher loading in the PHAT. Compared to the PHAT, the presence of randomly oriented fibers and homogeneous distribution of nHA particles in the PHA1 caused the highest percentage elongation [58]. Despite having a random orientation, PHA2 electrospun fibers showed a reduced percentage elongation and possessed a moderate tensile strength when compared to other electrospun composite samples. It may be due to the agglomeration of highly loaded

nHA nanoparticles. The optimized PHAT showed a significant elongation at break of 355% and the lowest Young's modulus of 0.0205 MPa (Fig. 5d), which shows the high flexibility of the PHAT composite [59]. So, it is a promising material for the fabrication of flexible piezoelectric nanogenerators.

Dielectric and piezoelectric properties

The following equation defines dielectric permittivity [42].

$$\varepsilon(\omega) = \varepsilon'(\omega) - i\varepsilon''(\omega) \quad (1)$$

where $\varepsilon''(\omega)$ represents the imaginary part of the permittivity, ω is the angular frequency, and $\varepsilon'(\omega)$ denotes the real part of the dielectric permittivity. The real part belongs to the interfacial polarization in the polymer composites, and the imaginary part is attributed to the dielectric loss ($\tan \delta$) [42]. Charges accumulate between the polymer matrix and conductive fillers in a polymer composite due to the Maxwell–Wagner–Sillars effect, resulting in major polarization [60].

The relative permittivity (ε') of PU, PHA1, PHA2, and PHAT at 20 Hz was found to be 1.96, 3.59, 4.18, and 28.44, respectively. The dielectric loss ($\tan \delta$) of PU, PHA1, PHA2, and PHAT at 20 Hz was found to be 0.096, 0.14, 0.15, and 5.88, respectively. As the filler amount was increased, permittivity and dielectric loss were gradually increased from pristine electrospun PU to PHAT samples. The incorporation of nHA into the PHA1 and PHA2 samples and nHA/o-MWCNT hybrid filler into the PHAT sample was responsible for the dielectric value improvement. The significant dielectric value in the pristine electrospun PU was attributed to the presence of dipole polarization of functional groups in the hard segments [41]. In the electrospun composite samples (PHA1 and PHA2), the improved permittivity was due to the originated interfacial and orientation polarization upon increasing the amount of nHA filler. The interfacial polarization is due to the heterogeneity between the polymer matrix (PU) and fillers (nHA and o-MWCNT) (Maxwell Wagner effect). The orientation polarization is due to the polar nature of the nanohydroxyapatite filler. Apart from the interfacial and orientation polarizations, the large dielectric value of the PHAT sample was due to the presence of axially aligned o-MWCNT along the electrospun fibers. A TEM micrograph is shown in Fig. S6.

MWCNT, or o-MWCNT, is the most widely used conductive filler to enhance the dielectric properties due to its large aspect ratio, good electrical conductivity, and unique mechanical properties [61].

The frequency dependency on the dielectric characteristics of materials is one of the essential factors for its widespread application. Figure 6a and b shows the variation of dielectric constant (ε') and dielectric loss ($\tan \delta$) of various samples in the frequency range of 20 Hz to 10 MHz. At lower frequencies, ε' was found to be high and decreased gradually as the frequency was increased. At lower frequencies, developed dipoles can align in the direction of the applied field, leading to higher permittivity. As the frequency increases, dipoles do not get enough time to align with the externally applied field, decreasing dielectric permittivity [41]. The dielectric loss of every electrospun membrane decreased gradually as the frequency was increased. It showed a stable $\tan \delta$ value between 10^3 and 10^4 Hz. After 10^4 Hz, the dielectric loss of PU, PHA1, and PHA2 increased. But for PHAT, the dielectric loss was increased only after $10^{6.5}$ Hz (Fig. 6b inset). It was due to the enhanced dipole polarization relaxation of MWCNT at 1.09 GHz compared to the nHA and the PU [62]. So, sample PHAT is considered a promising material with good dielectric properties for allied applications.

The ferro-piezoelectric characteristics of the electrospun membranes were investigated by DC-EFM analysis. The topographic features were captured, as shown in Fig. S7. The EFM signals were recorded between the voltages of +10 V and –10 V. The bias voltage was applied as follows: start from 0 to +10 V and then reverse to 0 V; subsequently, sweep to –10 V and then return to 0 V. Figure 6c shows the trend of the DC-EFM amplitude signal versus applied voltage for pristine electrospun PU and nHA-filled composites. The butterfly-shaped EFM amplitude curve indicated the existence of a ferro-piezoelectric material [63]. The less prominent pattern of the amplitude curve of the PU suggested the absence or lesser prominence of the ferro-piezoelectric features. In nHA-filled composites, the butterfly-like shape of the amplitude signal became prominent as the applied bias advanced in both directions. This observation supported the establishment of the piezoelectric feature in the PU-based composites containing nHA filler. Inclusion of nHA could generate a large number of internal dipoles in the composites, which was responsible for the observed

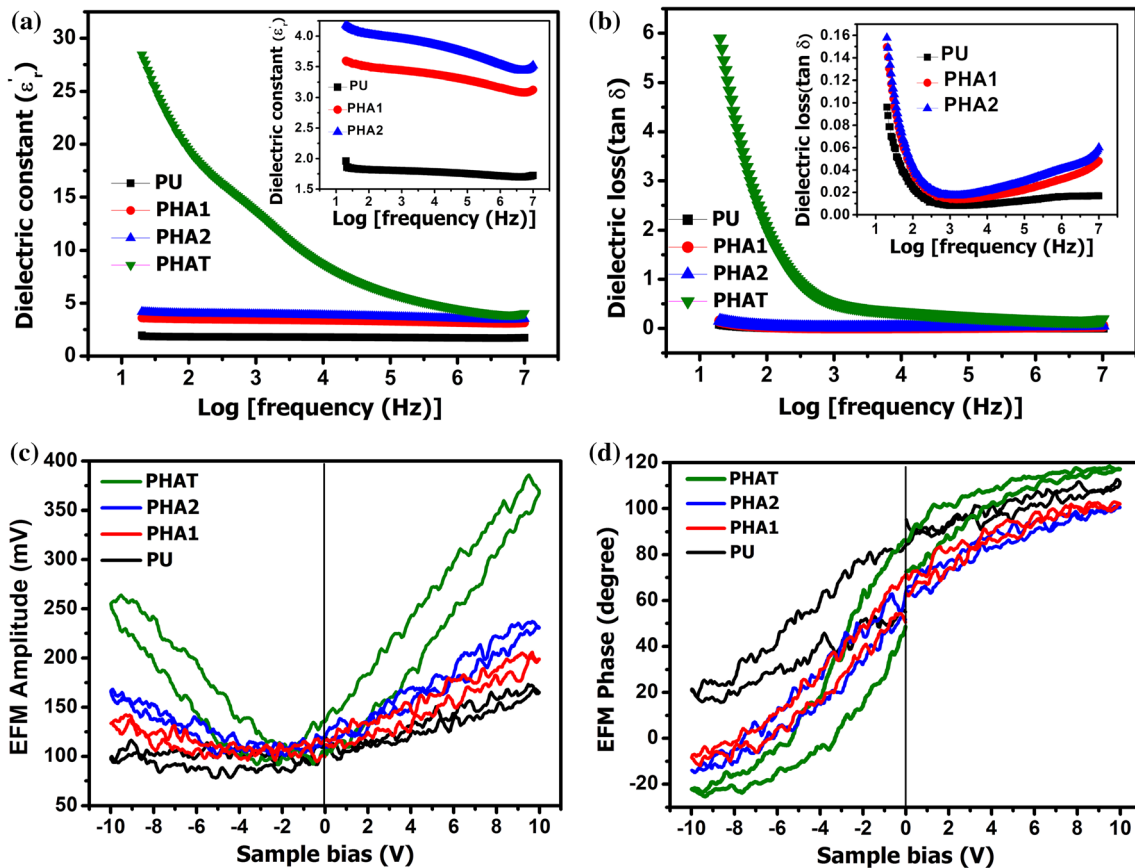


Figure 6 a Variation of dielectric constant of samples, b variation of dielectric loss of samples, c DC-EFM amplitude curves of samples, d DC-EFM phase curves of samples.

piezoelectric properties. The most prominent amplitude signal was observed for the PHAT composite due to the presence of enhanced electrical conductivity and polarization processes [64]. The EFM amplitude reflects the strain experienced on the cantilever by virtue of the piezoelectric property of composites. Upon realigning the internal dipoles with the external bias, a strain is developed within the material, which subsequently enhances the EFM amplitude [65]. Upon retracing, the signal follows a different path due to the remnant polarization. Figure 6d represents the EFM phase hysteresis signals, which indicate the ability of dipoles within the composites to undergo orientation switching with the direction of applied bias. Essentially, the orientation switching of the dipoles indicates the ferroelectric nature of the composites [66]. The phase hysteresis curve also shows the polarization reversal property at an applied voltage of ± 10 V. The PHAT composite showed a well-defined phase hysteresis curve, which can be accounted for by the generation of a large

number of dipoles with the ability to switch their orientation with the external bias easily. So, it confirmed the piezoelectric nature of electrospun composite membranes.

Piezoelectric nanogenerator performance test

To explore the piezoelectric voltage generating capacity of composite systems, piezoelectric nanogenerators (PENGs) were developed, and the output voltage was recorded under various stimuli. Initially, the devices were subjected to an impact force test with an impact force of 1.73 N to demonstrate the energy harvesting performance with controlled tapping force and area. A video showing the output voltage during the impact force test is given under Supplementary video SV1.

Figure 7 shows the output voltage generated by each device. It showed a damping trend in the curves. At the moment of impact, potential energy

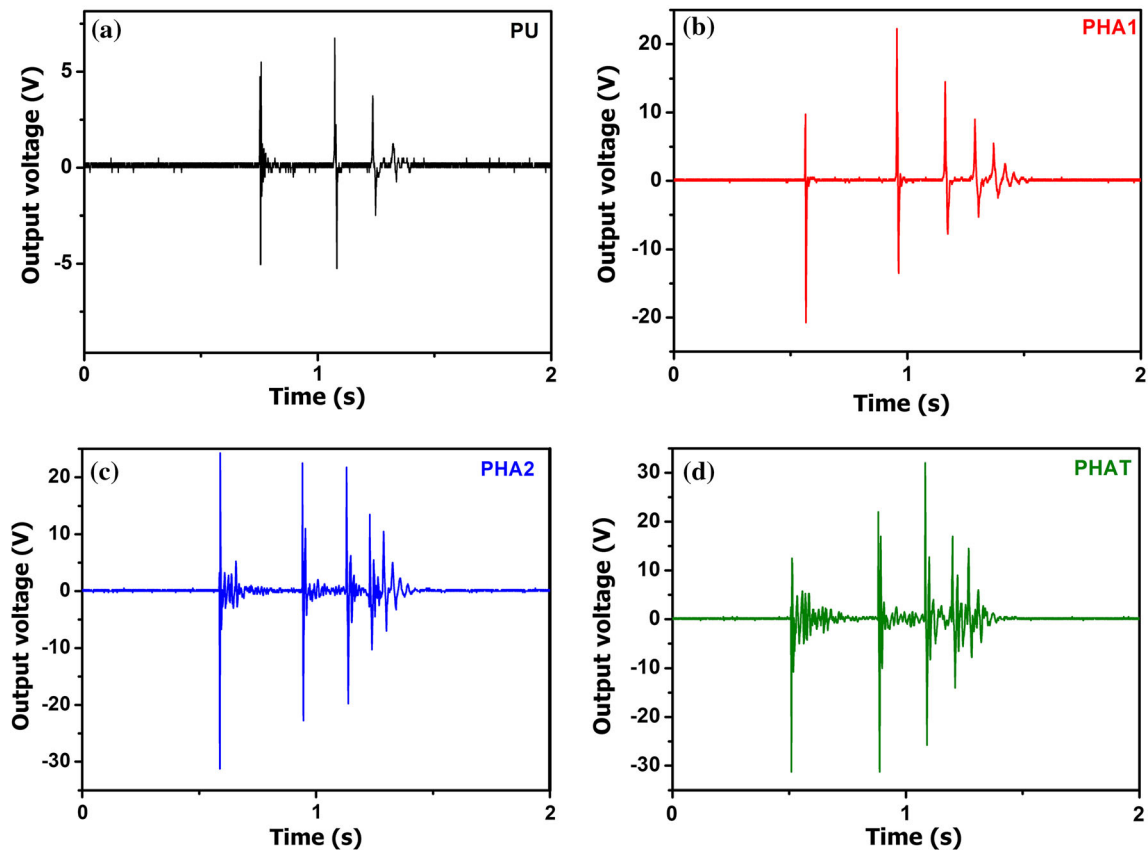


Figure 7 Output voltage generated by samples due to the impact force of 1.73 N **a** electrospun PU, **b** PHA1, **c** PHA2, **d** PHAT.

was converted to electrical energy, generating a peak voltage; however, some energy was lost due to damping. The peak-to-peak output voltages were 15.5 V, 47.5 V, 55.5 V, and 63.25 V, respectively, for neat PU, PHA1, PHA2, and PHAT devices. The maximum output voltage was recorded as 5.75 V, 22.25 V, 24.25 V, and 32 V for PU, PHA1, PHA2, and PHAT, respectively. It was observed that the output voltage increased gradually with the increase in the amount of nHA filler. However, the unfilled PU generated an output voltage despite its non-piezoelectric nature. It may be mainly due to the triboelectric voltage generated by friction between the polymer mat and the electrodes.

An impact test from a tapping machine was performed to examine the energy harvesting during a continuous impact other than an immediate impact with a controlled tapping frequency. A video showing the output voltage generation from a tapping machine is given under Supplementary video SV2. Figure 8 shows the output voltage generated by each device. It offered continuous positive and negative

peaks without damping due to the regular, periodic tapping.

The maximum output voltage was recorded as 1.25 V, 4.20 V, 5.20 V, and 7.5 V for PU, PHA1, PHA2, and PHAT, respectively. The amount of nHA in the composite samples (PHA1 and PHA2) increased, and the output voltage also increased. The highest output voltage in the PHAT sample was due to the presence of hybrid nHA/o-MWCNT filler. The pristine PU sample showed less intense and irregular peaks. On the other hand, all the composite samples showed sharp peaks due to the enhanced output voltage, which is attributed to the combined effect of piezoelectricity and a small fraction of triboelectricity. Moreover, a delay between two consecutive peaks confirmed the contribution of triboelectricity to the net output voltage [67].

Due to daily activity, the human body produces a significant amount of mechanical energy, which could be a promising energy source for energy harvesting from piezoelectric materials [68]. Moreover, the ability of piezoelectric materials to respond to

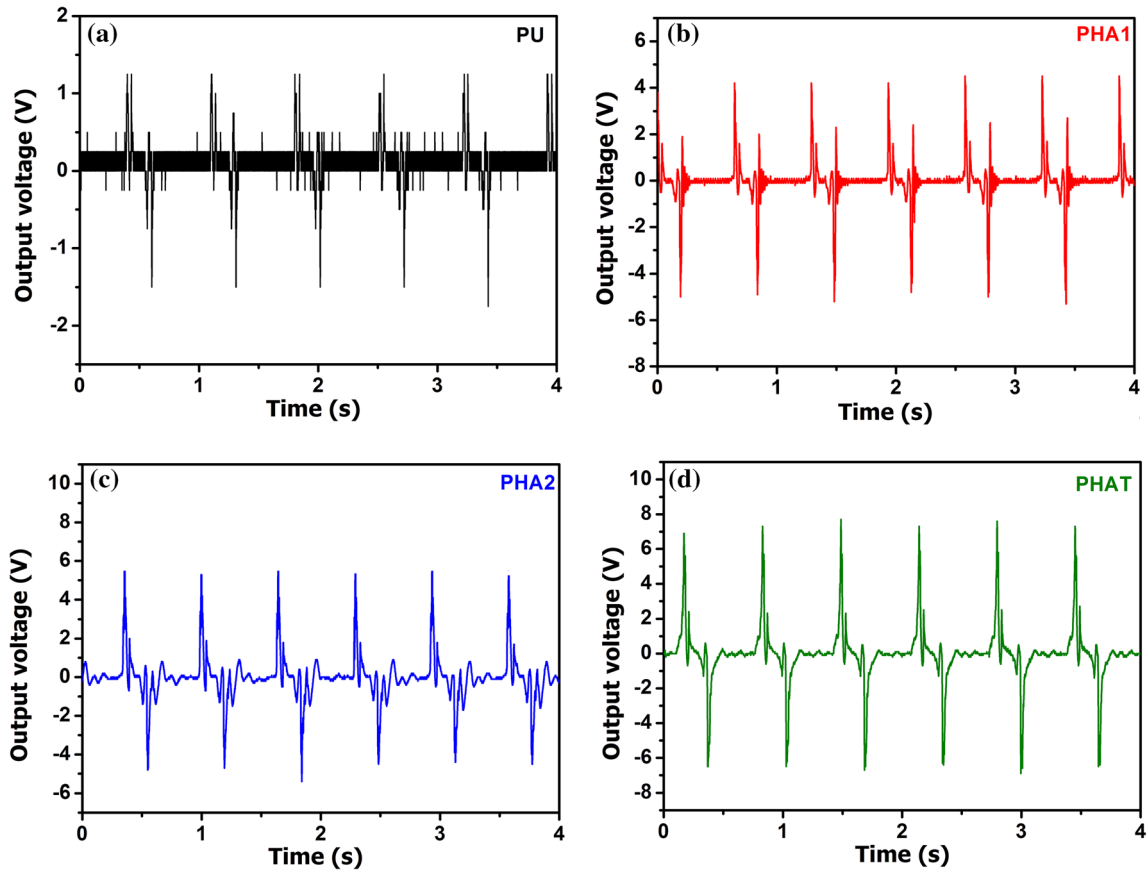


Figure 8 The output voltage of samples during continuous constant impact (frequency controlled) from a tapping machine **a** electrospun PU, **b** PHA1, **c** PHA2, **d** PHAT.

various motions is a crucial property for using them as devices to track the movement of joints in the human body during sports activities [69, 70]. In this scenario, piezoelectric power generated from piezoelectric materials triggered by human body motions can be considered an energy harvesting process and body motion-sensing strategy. The devices have been subjected to stimuli-responsive output voltage production from finger tapping, palm-bending motion, elbow joint motion, foot tapping, and throat muscle motion of an adult human to validate the performance of the various PU-based piezoelectric nanogenerators (PENGs) under various human body motions.

Figure 9 shows the output voltage generated from various PU-based PENGs under different human body-based mechanical stimuli. Figure 9a shows the output voltage generated from the periodic compressive forces through a human finger-tapping process. The observed output voltages were 2.2 V, 6.75 V, 9.25 V, and 23.25 V for neat PU, PHA1, PHA2,

and PHAT devices, respectively. Complementary to the EFM amplitude results, a drastic enhancement in the output voltage was observed for the PHAT composite containing nHA/o-MWCNT. It could be accounted for by the enhanced electron transport through the composite due to the o-MWCNT addition. The higher conductivity could improve the surface charge density of the composite, supporting better piezoelectric performance. Also, the composite's conductivity enhancement would help in the easy conduction of generated piezoelectricity [29]. In the output voltage signal, there is a well-defined fluctuation between a positive and a negative peak, which corresponds to the flow of electrons back and forth in the circuit as a result of the alternation of piezoelectric charge polarization [71].

A palm-bending motion-responsive output voltage analysis was performed on various PENGs to investigate the effect of human body bending motions on voltage production. Substantial output voltages were observed from the device upon bending activities.

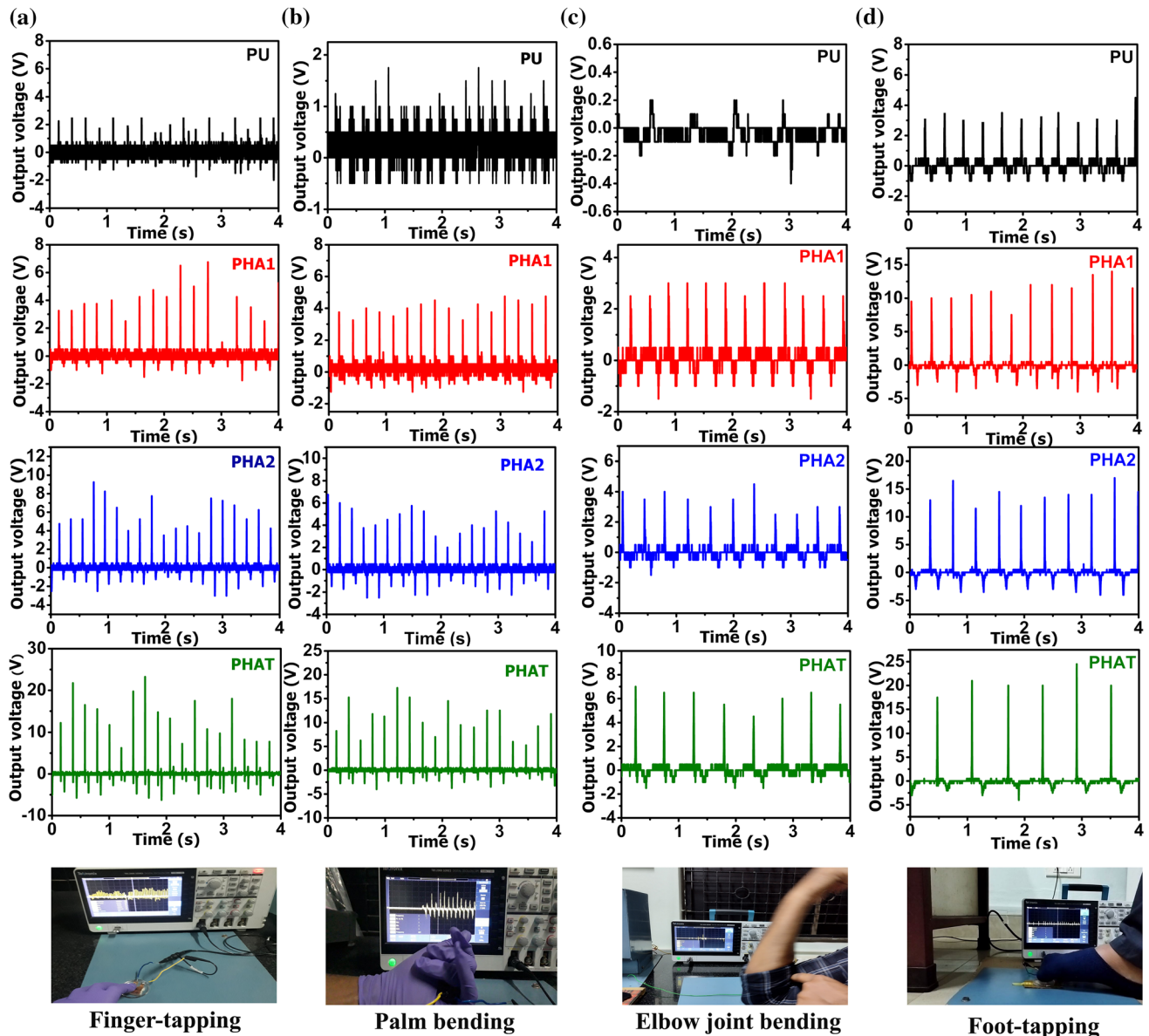


Figure 9 The digital photographs and output voltage generated by PU-based piezoelectric nanogenerators under various human body movements **a** finger tapping, **b** palm bending, **c** elbow joint bending motions, **d** foot tapping.

The output voltages during human palm bending were 1.75 V, 4.4 V, 5.75 V, and 17.25 V, respectively, from PU, PHA1, PHA2, and PHAT devices (Fig. 9b). A video showing the output voltage during palm-bending motions is given under Supplementary video SV3. An elbow joint motion experiment was also performed to complement the bending motion-based energy harvesting. The observed voltages during elbow joint motions were 0.2 V, 3 V, 4.5 V, and 7 V, respectively, from PU, PHA1, PHA2, and PHAT devices (Fig. 9c). A video showing output voltage during elbow joint motion is given under

Supplementary video SV4. As expected, output voltage gradually increased from the PU to the PHAT sample for both palm and elbow joint bending motions.

A foot-tapping experiment was also conducted to examine the practical application of energy harvesting during human walking. The output voltages from PU, PHA1, PHA2, and PHAT were 2.5 V, 12.14 V, 16.5 V, and 24.4 V, respectively (Fig. 9d). As expected, a gradual increase in the output voltage was observed from PU to PHAT. A video showing the energy harvesting during foot tapping is given under

Supplementary video SV5. A throat muscle-responsive output voltage analysis was performed on various PENG samples to investigate the effect of sensitive human body motions on voltage production. The observed voltages during throat muscle motions were 0.08 V, 0.25 V, 0.3 V, and 0.4 V from PU, PHA1, PHA2, and PHAT devices, respectively (Fig.S8). Since the stimulation of throat muscle is deficient compared to all other body stimuli, the lowest output voltage was observed. Overall, the human body's stimuli-responsive output voltages were recorded as 0.4 V, 7 V, 17.25 V, 23.25 V, and 24.4 V, respectively, for throat muscle motion, elbow joint bending, palm bending, finger tapping, and foot tapping from the PHAT sample. So, as the human body's impact increases, output voltage also increases.

Finger-tapping and machine tapping experiments were used to evaluate the current (I), power (P), current density (J), and power density (P_d) of the PU-based composite. During the experiment, a resistor of 1 M Ω was attached to the circuit. Figure S9 shows the output voltage generated during the finger-tapping experiment. It was observed that the closed-circuit current increased, with a similar trend to that observed in the previous experiments. But relatively, the output voltages were decreased compared to the resistance-free energy harvesting. This reduction was due to a 1-M Ω resistor in the circuit. The highest circuit current of the PHAT sample was owing to the conductive hybrid filler (nHA/o-MWCNT). The power density of devices also increased with filler inclusion, and the highest power density was recorded for the composite PHAT containing o-MWCNT. The voltage, current, and power characteristics of devices under different mechanical stimuli are

tabulated in Table 3. The ability of the PU-based composites to generate a piezoelectric voltage in various environments demonstrates their versatility for energy generation and motion-sensing applications.

Flexible materials with high mechanical properties are essential for PENG fabrication to maintain long-term mechanical stability due to the mechanical impact imposed during energy harvesting. Table 4 shows a comparison of the current work with other reports on non-PVDF electrospun membrane-based piezoelectric nanogenerators. It shows that the present work can show high strength with high tensile strength and high flexibility due to significant percentage elongation; hence, it can tolerate the impact forces applied during energy harvest for an extended period. DC-EFM confirms the contribution of the piezoelectricity from the combined piezo-triboelectricity produced from composite-based PENGs. Compared to other studies, the present work explores piezoelectric energy harvesting using human body stimuli such as finger tapping, elbow bending, palm bending, leg tapping, and throat motions. Moreover, it investigates impact force-controlled, frequency-controlled, and area-controlled energy harvestings. It shows a significantly higher output voltage compared to other materials. So, the PU-based electrospun composite membrane is a potential material for the development of piezoelectric and triboelectric nanogenerators.

Conclusions

A flexible PU electrospun composite membrane-based piezoelectric nanogenerator (PENG) has been fabricated as an alternative energy harvester. All

Table 3 Device performance parameters

Mechanical energy source	Samples	Output voltage (V)	Current (μ A)	Current density (μ A/ cm^2)	Power (μ W)	Power density (μ W/ cm^2)
Finger tapping	PU	1.4	1.4	0.35	1.95	0.49
	PHA1	2.2	2.2	0.55	4.84	1.21
	PHA2	2.7	2.7	0.675	7.29	1.82
	PHAT	3.9	3.9	0.975	15.21	3.80
Machine tapping	PU	0.76	0.76	0.19	0.577	0.144
	PHA1	1.47	1.47	0.367	2.16	0.5402
	PHA2	1.61	1.61	0.402	2.592	0.6480
	PHAT	1.95	1.95	0.487	3.80	0.9506

Table 4 Comparison of the piezoelectric performance of the present work with other non-PVDF-based piezoelectric nanogenerators

Material	Maximum output voltage (V)	Mode of piezo-ferroelectric properties evaluation	Mode of energy harvesting	Mechanical properties		References
				Tensile strength (MPa)	Elongation at break (%)	
EVA-MPU/nHA	1.39	DC-EFM analysis	FT, EB, and TM	2.9	N.R	[37]
PAN/CuO	5	N.R	FT and CTM	N.R	N.R	[36]
Silk nanofiber	7	P-E hysteresis analysis	EB and LT	N.R	N.R	[72]
Casein/polyvinyl alcohol	20	P-E hysteresis analysis	FT and CTM	2.95	154	[73]
PAN/ZnO	8.17	N.R	W and R	N.R	N.R	[74]
PU/nHA@o-MWCNT	32	DC-EFM analysis	FT, PB, EB, TM,LT,W, CIF, and CTM	10.11	355	This study

DC-EFM Dynamic-contact electrostatic force microscopy, *FT* finger tapping, *PB* palm bending, *EB* elbow bending, *TM* throat motion, *LT* leg tapping, *W* walking, *R* running, *CIF* controlled impacting force, *CTM* controlled tapping machine, *N.R* not reported

electrospun composite membranes outperformed the pristine PU nanofibrous membrane in mechanical and thermal properties. The nHA/o-MWCNT hybrid filler-modified sample (PHAT) showed a significant percentage elongation (355%) and the lowest Young's modulus, which correlates with the high flexibility. Compared to the pristine PU nanofibrous membrane, composite electrospun membranes exhibited improvements in ferro-piezoelectric properties and dielectric properties. The EFM amplitude signals showed a butterfly loop, and the EFM phase signals exhibited hysteresis curves for all composites, which confirmed the piezoelectricity. The dielectric properties were found to increase with filler loading and decrease with an increase in the external field frequency. Outstanding improvements in the dielectric and piezoelectric properties were observed for the PHAT composite fibrous membrane. PHAT-based PENG showed the highest output voltage during the impact force (32 V) and human body motion stimuli-responsive tests (24.4 V) compared to the pristine PU-based PENG. So, the flexible polyurethane-based electrospun composite membrane is a potential material for the development of piezoelectric nanogenerators and can open up a new spectrum of opportunities in the field of energy harvesting.

Acknowledgements

The authors gratefully acknowledge CeNSE, Bangalore, for FESEM analysis.

Author contributions

KJ helped in conceptualization (lead), methodology (lead), investigation (lead), and writing original draft (lead). SVH contributed to investigation and writing (supporting). AMC and PKSM investigated the study (supporting). SV performed supervision (equal), review and editing (supporting). AS was involved in supervision (lead), conceptualization (equal), review, and editing (equal).

Data availability

All data generated or analyzed during this study are included in this published article (and its supplementary information files).

Declarations

Conflict of interest The authors hereby declare that there is no conflict of interest and satisfy all ethics in publishing policy.

Supplementary Information: The online version contains supplementary material available at <http://doi.org/10.1007/s10853-022-08086-8>.

References

- [1] Stoica D, Alexe P, Ivan AS, Moraru DI, Ungureanu CV, Stanciu S, and Stoica M (2022) Biopolymers: global carbon footprint and climate change. In: *Biopolymers* (pp. 35–54). Springer, Cham
- [2] Mohsin M, Bashir S, Baloch ZA, Hafeez M (2022) Assessment of sustainability and uncertainties of oil markets: mediating determinants of energy use and CO₂ emissions. *Environ Sci Pollut Res* 29(1):663–676
- [3] Zhang Y, Abbas M, Iqbal W (2022) Perceptions of GHG emissions and renewable energy sources in Europe Australia and the USA. *Environ Sci Pollut Res* 29(4):5971–5987
- [4] Sessini V, Thai CN, Amorín H, Jiménez R, Samuel C, Caillol S, Cornil J, Hoyas S, Barrau S, Dubois P (2021) Solvent-free design of biobased non-isocyanate polyurethanes with ferroelectric properties. *ACS Sustain Chem Eng* 9(44):14946–14958
- [5] Fu G, He Y, Liang Y, He S, Xue R, Wu Y, Yu W, Shi Q (2022) Enhanced piezoelectric performance of rare earth complex-doped sandwich-structured electrospun P (VDF-HFP) multifunctional composite nanofiber membranes. *J Mater Sci: Mater Electron* 33:22183–22195. <https://doi.org/10.1007/s10854-022-08998-w>
- [6] Sampson JC, Batra A, Edwards ME, Kotru S, Bowen CR, Vaseashta A (2022) On the mechanisms of DC conduction in electrospun PLZT/PVDF nanocomposite membranes. *J Mater Sci* 57(8):5084–5096. <https://doi.org/10.1007/s10853-022-06958-7>
- [7] Mohanta MK, Rawat A, Jena N, Ahammed R, De Sarkar A (2020) Superhigh flexibility and out-of-plane piezoelectricity together with strong anharmonic phonon scattering induced extremely low lattice thermal conductivity in hexagonal buckled CdX (X= S, Se) monolayers. *J Phys: Condens Matter* 32(35):355301
- [8] Ma SW, Fan YJ, Li HY, Su L, Wang ZL, Zhu G (2018) Flexible porous polydimethylsiloxane/lead zirconate titanate-based nanogenerator enabled by the dual effect of ferroelectricity and piezoelectricity. *ACS Appl Mater Interfaces* 10(39):33105–33111
- [9] Banerjee S, Bairagi S, Ali SW (2021) A critical review on lead-free hybrid materials for next generation piezoelectric energy harvesting and conversion. *Ceram Int* 47(12):16402–16421
- [10] He H, Lu W, Oh JAS, Li Z, Lu X, Zeng K, Lu L (2020) Probing the coexistence of ferroelectric and relaxor states in Bi0.5Na0.5TiO₃-based ceramics for enhanced piezoelectric performance. *ACS Appl Mater Interfaces* 12(27):30548–30556
- [11] Liu Y, Khanbareh H, Halim MA, Feeney A, Zhang X, Heidari H, Ghannam R (2021) Piezoelectric energy harvesting for self-powered wearable upper limb applications. *Nano Select* 2(8):1459–1479
- [12] Martins P, Costa CM, Botelho G, Lanceros-Mendez S, Barandiaran J, Gutierrez J (2012) Dielectric and magnetic properties of ferrite/poly (vinylidene fluoride) nanocomposites. *Mater Chem Phys* 131(3):698–705
- [13] Surmenev RA, Orlova T, Chernozem RV, Ivanova AA, Bartasyte A, Mathur S, Surmeneva MA (2019) Hybrid lead-free polymer-based nanocomposites with improved piezoelectric response for biomedical energy-harvesting applications: a review. *Nano Energy* 62:475–506
- [14] Saxena P, Shukla P (2021) A comprehensive review on fundamental properties and applications of poly (vinylidene fluoride)(PVDF). *Adv Compos Hybrid Mater* 4(1):8–26
- [15] Fan FR, Tang W, Wang ZL (2016) Flexible nanogenerators for energy harvesting and self-powered electronics. *Adv Mater* 28(22):4283–4305
- [16] Shao H, Fang J, Wang H, Lin T (2015) Effect of electrospinning parameters and polymer concentrations on mechanical-to-electrical energy conversion of randomly-oriented electrospun poly (vinylidene fluoride) nanofiber mats. *RSC Adv* 5(19):14345–14350
- [17] Ke K, McMaster M, Christopherson W, Singer KD, Manas-Zloczower I (2019) Effects of branched carbon nanotubes and graphene nanoplatelets on dielectric properties of thermoplastic polyurethane at different temperatures. *Compos B Eng* 166:673–680
- [18] Yu C-T, Lai C-C, Wang F-M, Liu L-C, Liang W-C, Wu C-L, Chiu J-C, Liu H-C, Hsiao H-T, Chen C-M (2019) Fabrication of thermoplastic polyurethane (TPU)/thermoplastic amide elastomer (TPAE) composite foams with supercritical carbon dioxide and their mechanical properties. *J Manuf Process* 48:127–136
- [19] Thomas B, Raj MC, Joy J, Moores A, Drisko GL, Sanchez C (2018) Nanocellulose, a versatile green platform: from bio-sources to materials and their applications. *Chem Rev* 118(24):11575–11625
- [20] Xue B, Zhang F, Zheng J, Xu C (2021) Flexible piezoelectric device directly assembled through the continuous electrospinning method. *Smart Mater Struct* 30(4):045006. <https://doi.org/10.1088/1361-665X/abe3a8>
- [21] Yu S, Tai Y, Milam-Guerrero J, Nam J, Myung NV (2022) Electrospun organic piezoelectric nanofibers and their energy

- and bio applications. *Nano Energy* 97:107174. <https://doi.org/10.1016/j.nanoen.2022.107174>
- [22] Sengupta A, Das S, Dasgupta S, Sengupta P, Datta P (2021) Flexible nanogenerator from electrospun PVDF–polycarbazole nanofiber membranes for human motion energy-harvesting device applications. *ACS Biomater Sci Eng* 7(4):1673–1685
- [23] Khalifa M, Mahendran A, Anandhan S (2019) Durable, efficient, and flexible piezoelectric nanogenerator from electrospun PANi/HNT/PVDF blend nanocomposite. *Polym Compos* 40(4):1663–1675
- [24] Lu L, Ding W, Liu J, Yang B (2020) Flexible PVDF based piezoelectric nanogenerators. *Nano Energy* 78:105251. <http://doi.org/10.1016/j.nanoen.2020.105251>
- [25] Rodriguez R, Rangel D, Fonseca G, Gonzalez M, Vargas S (2016) Piezoelectric properties of synthetic hydroxyapatite-based organic-inorganic hydrated materials. *Results in Physics* 6:925–932
- [26] Haojie D, Liuyun J, Bingli M, Shengpei S (2018) Preparation of a highly dispersed nanohydroxyapatite by a new surface-modification strategy used as a reinforcing filler for poly(lactic-co-glycolide). *Ind Eng Chem Res* 57(50):17119–17128
- [27] Li B, Guo B, Fan H, Zhang X (2008) Preparation of nanohydroxyapatite particles with different morphology and their response to highly malignant melanoma cells in vitro. *Appl Surf Sci* 255(2):357–360
- [28] Abidi SSA, Murtaza Q (2014) Synthesis and characterization of nano-hydroxyapatite powder using wet chemical precipitation reaction. *J Mater Sci Technol* 30(4):307–310. <https://doi.org/10.1016/j.jmst.2013.10.011>
- [29] Shafeeq VH, Subash CK, Varghese S, Unnikrishnan GP (2020) Nanohydroxyapatite embedded blends of ethylene-co-vinyl acetate and millable polyurethane as piezoelectric materials: dielectric, viscoelastic and mechanical features. *Polym Int* 69(12):1256–1266
- [30] Galindo TGP, Chai Y, Tagaya M (2019) Hydroxyapatite nanoparticle coating on polymer for constructing effective biointeractive interfaces. *J Nanomater* 2019:6495239. <http://doi.org/10.1155/2019/649523932>
- [31] Kim MP, Um D-S, Shin Y-E, Ko H (2021) High-performance triboelectric devices via dielectric polarization: a review. *Nanoscale Res Lett* 16(1):1–14
- [32] Mokhtari F, Azimi B, Salehi M, Hashemikia S, Danti S (2021) Recent advances of polymer-based piezoelectric composites for biomedical applications. *J Mech Behav Biomed Mater* 122:104669. <https://doi.org/10.1016/j.jmbbm.2021.104669>
- [33] Liu Q, Zhu J, Zhang L, Qiu Y (2018) Recent advances in energy materials by electrospinning. *Renew Sustain Energy Rev* 81:1825–1858
- [34] Xue J, Xie J, Liu W, Xia Y (2017) Electrospun nanofibers: new concepts, materials, and applications. *Acc Chem Res* 50(8):1976–1987
- [35] Sun B, Li X, Zhao R, Ji H, Qiu J, Zhang N, He D, Wang C (2019) Electrospun poly (vinylidene fluoride)-zinc oxide hierarchical composite fiber membrane as piezoelectric acoustoelectric nanogenerator. *J Mater Sci* 54(3):2754–2762. <https://doi.org/10.1007/s10853-018-2985-x>
- [36] Bairagi S, Chowdhury A, Banerjee S, Thakre A, Saini A, Ali SW, (2022) Investigating the role of copper oxide (CuO) nanorods in designing flexible piezoelectric nanogenerator composed of polyacrylonitrile (PAN) electrospun web-based fibrous material. *J Mater Sci: Mater Electron* 33:13152–13165. <https://doi.org/10.1007/s10854-022-08254-1>
- [37] Shafeeq VH, Karumuthil SC, Juraij K, Varghese S, Athiyathil S, Panicker UG (2021) Stimuli-responsive electrospun piezoelectric mats of ethylene-co-vinyl acetate-millable polyurethane–nanohydroxyapatite composites. *ACS Appl Mater Interfaces* 13(20):24106–24116
- [38] Liu S, Sun H, Ning N, Zhang L, Tian M, Zhu W, Chan TW (2016) Aligned carbon nanotubes stabilized liquid phase exfoliated graphene hybrid and their polyurethane dielectric elastomers. *Compos Sci Technol* 125:30–37
- [39] Mi H-Y, Li Z, Turng L-S, Sun Y, Gong S (2014) Silver nanowire/thermoplastic polyurethane elastomer nanocomposites: thermal, mechanical, and dielectric properties. *Mater Des* 1980–2015(56):398–404
- [40] He X, Zhou J, Jin L, Long X, Wu H, Xu L, Gong Y, Zhou W (2020) Improved dielectric properties of thermoplastic polyurethane elastomer filled with Core-Shell structured PDA@ TiC particles. *Materials* 13(15):3341. <https://doi.org/10.3390/ma13153341>
- [41] Variar L, Muralidharan MN, Narayanankutty SK, Ansari S (2021) High dielectric constant, flexible and easy-processable calcium copper titanate/thermoplastic polyurethane (CCTO/TPU) composites through simple casting method. *J Mater Sci: Mater Electron*. 32:5908–5919. <https://doi.org/10.1007/s10854-021-05311-z>
- [42] Jun Y-S, Habibpour S, Hamidinejad M, Park MG, Ahn W, Yu A, Park CB (2021) Enhanced electrical and mechanical properties of graphene nano-ribbon/thermoplastic polyurethane composites. *Carbon* 174:305–316
- [43] Fernando MS, Wimalasiri A, Dziemidowicz K, Williams GR, Koswattage K, Dissanayake D, de Silva KN, de Silva RM (2021) Biopolymer-based nanohydroxyapatite composites for the removal of fluoride lead, cadmium, and arsenic from water. *ACS omega* 6(12):8517–8530
- [44] Venkatesan M, Chen W-C, Cho C-J, Veeramuthu L, Chen L-G, Li K-Y, Tsai M-L, Lai Y-C, Lee W-Y, Chen W-C

- (2022) Enhanced piezoelectric and photocatalytic performance of flexible energy harvester based on CsZn_{0.75}Pb_{0.25}I₃/CNC–PVDF composite nanofibers. *Chem Eng J* 433:133620. <https://doi.org/10.1016/j.cej.2021.133620>
- [45] Juraij K, Chingakham C, Manaf O, Sagitha P, Suni V, Sajith V, Sujith A (2022) Polyurethane/multi-walled carbon nanotube electrospun composite membrane for oil/water separation. *J Appl Polym Sci* 139(19):52117. <https://doi.org/10.1002/app.52117>
- [46] Ma S, Ye T, Zhang T, Wang Z, Li K, Chen M, Zhang J, Wang Z, Ramakrishna S, Wei L (2018) Highly oriented electrospun P (VDF-TrFE) fibers via mechanical stretching for wearable motion sensing. *Adv Mater Technol* 3(7):1800033. <https://doi.org/10.1002/admt.201800033>
- [47.] Zaarour B, Zhu L, Huang C, Jin X (2019) Enhanced piezoelectric properties of randomly oriented and aligned electrospun PVDF fibers by regulating the surface morphology. *J Appl Polym Sci* 136(6):47049. <https://doi.org/10.1002/app.47049>
- [48] Kandiyil J, Vasudevan S, Athiyannathil S (2022) Efficient selective methylene blue adsorption by polyurethane/montmorillonite-based antifouling electrospun composite membranes. *J Appl Polym Sci*. <https://doi.org/10.1002/app.53464>
- [49] Meskinfam M, Bertoldi S, Albanese N, Cerri A, Tanzi MC, Imani R, Baheiraei N, Farokhi M, Fare S (2018) Polyurethane foam/nano hydroxyapatite composite as a suitable scaffold for bone tissue regeneration. *Mater Sci Eng, C* 82:130–140
- [50] Mirza S, Jolly R, Zia I, Saad Umar M, Owais M, Shakir M (2020) Bioactive gum Arabic/κ-carrageenan-incorporated nano-hydroxyapatite nanocomposites and their relative biological functionalities in bone tissue engineering. *ACS Omega* 5(20):11279–11290
- [51] Nara M, Morii H, Tanokura M (1828) (2013) Coordination to divalent cations by calcium-binding proteins studied by FTIR spectroscopy. *Biochim et Biophys Acta (BBA) - Biomembr* 10:2319–2327
- [52] Li L, Zuo Y, Zou Q, Yang B, Lin L, Li J, Li Y (2015) Hierarchical structure and mechanical improvement of an n-HA/GCO–PU composite scaffold for bone regeneration. *ACS Appl Mater Interfaces* 7(40):22618–22629
- [53] Aldosari MA, Othman AA, Alsharaeh EH (2013) Synthesis and characterization of the in situ bulk polymerization of PMMA containing graphene sheets using microwave irradiation. *Molecules* 18(3):3152–3167
- [54] Gomes AD, de Oliveira AA, Houmard M, Nunes EH (2021) Gamma sterilization of collagen/hydroxyapatite composites: validation and radiation effects. *Appl Radiat Isot* 174:109758. <https://doi.org/10.1016/j.apradiso.2021.109758>
- [55] Sundaran SP, Reshmi CR, Sagitha P, Sujith A (2020) Polyurethane nanofibrous membranes decorated with reduced graphene oxide–TiO₂ for photocatalytic templates in water purification. *J Mater Sci* 55(14):5892–5907. <https://doi.org/10.1007/s10853-020-04414-y>
- [56] Reshmi C, Sundaran SP, Juraij A, Athiyannathil S (2017) Fabrication of superhydrophobic polycaprolactone/beeswax electrospun membranes for high-efficiency oil/water separation. *RSC Adv* 7(4):2092–2102
- [57] Pedicini A, Farris RJ (2003) Mechanical behavior of electrospun polyurethane. *Polymer* 44(22):6857–6862
- [58] Eun JH, Sung SM, Kim MS, Choi BK, Lee JS (2021) Effect of MWCNT content on the mechanical and piezoelectric properties of PVDF nanofibers. *Mater Des* 206:109785. <https://doi.org/10.1016/j.matdes.2021.109785>
- [59] Wanasekara ND, Matolyak LE, Korley LTJ (2015) Tunable mechanics in electrospun composites via hierarchical organization. *ACS Appl Mater Interfaces* 7(41):22970–22979
- [60] Pvs HP, Jayamani E, Soon KH, Wong YC, Rahman MR, Bakri MKB (2021) Interfacial polarization effects on dielectric properties in flax reinforced polypropylene/strontium titanate composites. *Mater Chem Phys* 265:124489. <https://doi.org/10.1016/j.matchemphys.2021.124489>
- [61] Tao J, Cao S-A (2020) Flexible high dielectric thin films based on cellulose nanofibrils and acid oxidized multi-walled carbon nanotubes. *RSC Adv* 10(18):10799–10805
- [62] Hu H, Zheng Y, Ren K, Wang J, Zhang Y, Zhang X, Che R, Qin G, Jiang Y (2021) Position selective dielectric polarization enhancement in CNT based heterostructures for highly efficient microwave absorption. *Nanoscale* 13(4):2324–2332
- [63] Cherumannil Karumuthil S, Prabha Rajeev S, Valiyaneerilakkal U, Athiyannathil S, Varghese S (2019) Electrospun poly (vinylidene fluoride-trifluoroethylene)-based polymer nanocomposite fibers for piezoelectric nanogenerators. *ACS Appl Mater Interfaces* 11(43):40180–40188
- [64] Karumuthil SC, Rajeev SP, Varghese S (2017) Piezo-tribo nanoenergy harvester using hybrid polydimethyl siloxane based nanocomposite. *Nano Energy* 40:487–494
- [65] Karumuthil SC, Rajeev SP, Varghese S (2019) Poly (vinylidene fluoride-trifluoroethylene)-ZnO nanoparticle composites on a flexible poly (dimethylsiloxane) substrate for energy harvesting. *ACS Appl Nano Mater* 2(7):4350–4357
- [66] He C, Wang Z, Li X, Yang X, Long X, Ye Z-G (2017) Self-polarized high piezoelectricity and its memory effect in ferroelectric single crystals. *Acta Mater* 125:498–505
- [67] Jung W-S, Kang M-G, Moon HG, Baek S-H, Yoon S-J, Wang Z-L, Kim S-W, Kang C-Y (2015) High output piezo/triboelectric hybrid generator. *Sci Rep* 5(1):1–6

- [68] Huang L, Lin S, Xu Z, Zhou H, Duan J, Hu B, Zhou J (2020) Fiber-based energy conversion devices for human-body energy harvesting. *Adv Mater* 32(5):1902034
- [69] Amjadi M, Yoon YJ, Park I (2015) Ultra-stretchable and skin-mountable strain sensors using carbon nanotubes–Ecoflex nanocomposites. *Nanotechnology* 26(37):375501. <https://doi.org/10.1088/0957-4484/26/37/375501>
- [70] Boland CS, Khan U, Backes C, O’Neill A, McCauley J, Duane S, Shanker R, Liu Y, Jurewicz I, Dalton AB (2014) Sensitive, high-strain, high-rate bodily motion sensors based on graphene–rubber composites. *ACS Nano* 8(9):8819–8830
- [71] Ghosh SK, Adhikary P, Jana S, Biswas A, Sencadas V, Gupta SD, Tudu B, Mandal D (2017) Electrospun gelatin nanofiber based self-powered bio-e-skin for health care monitoring. *Nano Energy* 36:166–175
- [72] Sohn C, Kim H, Han J, Lee K-T, Šutka A, Jeong CK (2022) Generating electricity from molecular bonding-correlated piezoresponse of biodegradable silk nanofibers. *Nano Energy* 103:107844
- [73] Bairagi S, Banerjee S, Kalyaniyan P, Dhanalakshmi G, Ali SW (2021) New Insights toward casein/polyvinyl alcohol electrospun nanofibrous webs as a piezoelectric-cum-triboelectric energy harvester. *ACS Appl Electron Mater* 3(10):4348–4361
- [74] Sun Y, Liu Y, Zheng Y, Li Z, Fan J, Wang L, Liu X, Liu J, Shou W (2020) Enhanced energy harvesting ability of ZnO/PAN hybrid piezoelectric nanogenerators. *ACS Appl Mater Interfaces* 12(49):54936–54945

Publisher’s Note Springer Nature remains neutral with regard to jurisdictional claims in published maps and institutional affiliations.

Springer Nature or its licensor (e.g. a society or other partner) holds exclusive rights to this article under a publishing agreement with the author(s) or other rightsholder(s); author self-archiving of the accepted manuscript version of this article is solely governed by the terms of such publishing agreement and applicable law.